Global particulate matter pool temporal variability over the SeaWiFS period (1997-2007)

Vincent Vantrepotte, Hubert Loisel, F. Mélin, D. Dessailly, Lucile Duforêt-Gaurier

Global particulate matter pool temporal variability over the SeaWiFS period (1997–2007)

V. Vantrepotte,[1] H. Loisel,[1] F. Mélin,[2] D. Desailly,[1] and L. Duforêt-Gaurier[1]

Received 17 November 2010; accepted 21 December 2010; published 25 January 2011.

[1] Major patterns of temporal variability associated with marine particulate backscattering coefficient at 490 nm ($b_{bp}(490)$, an indicator of the particulate organic carbon concentration) and particle backscattering spectral dependency γ (a proxy for the relative proportion between small and large particles) are investigated with a 10-year SeaWiFS series. Generally, the contribution of the seasonal cycle to the series variance has a similar spatial pattern for γ and the chlorophyll *a* concentration (Chl*a*). The spatial distribution of significant monotonic changes for γ and Chl*a* (reaching up to $\pm 5\%\ yr^{-1}$) is also comparable with opposite signs of the slope, indicating that inter-annual changes in Chl*a* and average particle size are often positively correlated. Conversely, spatial patterns of seasonality and trend found for $b_{bp}(490)$ often differ from those of Chl*a* and γ. Particularly, large seasonal signals for $b_{bp}(490)$ are seen poleward of 45° while high seasonality for Chl*a* and γ is found in two mid-latitude zonal belts (~20°–40° latitude). Significant changes in $b_{bp}(490)$ over the considered decade are much fewer and usually not significant in areas where strong positive or negative changes in Chl*a* have been detected. This suggests that the changes in phytoplankton have not been translated in terms of overall particle stock. **Citation:** Vantrepotte, V., H. Loisel, F. Mélin, D. Desailly, and L. Duforêt-Gaurier (2011), Global particulate matter pool temporal variability over the SeaWiFS period (1997–2007), *Geophys. Res. Lett.*, *38*, L02605, doi:10.1029/2010GL046167.

1. Introduction

[2] The suspended particulate matter (PM) pool in the open ocean is diversely composed of phytoplankton, heterotrophic organisms, viruses and organic detritus which relative proportion and size distribution may vary widely in space and time. Among properties characterizing the PM pool, the particle size distribution (PSD) provides relevant information on marine ecosystem structure and functioning, conditions the physical transport of particles (including their export to the deep ocean) and biogeochemical interactions, and is therefore crucial for modelling marine biogeochemical cycles [*Aumont et al.*, 2003]. However, knowledge on PM spatiotemporal variability and PSD is still very scarce. In that context, ocean color remote sensing is a valuable asset. Various approaches have been proposed to retrieve the concentration of particulate organic carbon (POC) from satellite observations [e.g. *Stramski et al.*, 1999; *Loisel et al.*, 2002]. Moreover, recent works have shown the potential of using the spectral slope (γ) of the satellite-derived backscattering coefficient due to particles b_{bp} for estimating qualitatively the relative proportion between small and large particles in the surface ocean [*Loisel et al.*, 2006] and parameterizing the PSD function [*Kostadinov et al.*, 2009].

[3] Satellite-derived data have been much used to study the main patterns of seasonality associated with the chlorophyll *a* concentration (Chl*a*) [*Yoder and Kennelly*, 2003; *Vantrepotte and Mélin*, 2009] and to identify inter-annual changes in the Chl*a* record, highlighting the possible impacts of climate oscillations on marine biology [*Behrenfeld et al.*, 2006; *Martinez et al.*, 2009]. Similarly, this study aims at characterizing the seasonal and trend patterns of b_{bp} at 490 nm and γ from the global SeaWiFS 10-year monthly data series, and to relate these patterns to those documented for Chl*a*.

2. Material and Methods

2.1. Ocean-Color Data

[4] The primary satellite products used in this study are the spectrum of normalized water-leaving radiance (L_{WN}) and Chl*a* derived from the SeaWiFS sensor (reprocessing 2009.1), which are mapped on 5'-resolution cylindrical equidistant grids for the period November 1997 to October 2007. The $b_{bp}(\lambda)$ coefficients are determined from $L_{WN}(\lambda)$ at 490, 510, and 555 nm using the model defined by *Loisel and Stramski* [2000] which performance has been evaluated against *in situ* data representative of various optical conditions [*Loisel et al.*, 2001]. Assuming a power law for the spectral shape of $b_{bp}(\lambda) \sim \lambda^{-\gamma}$, the spectral slope γ is estimated by linear regression of the log-transformed b_{bp} on wavelength λ. In agreement with theory and *in situ* measurements [*Reynolds et al.*, 2001], the spectral slope γ is sensitive to variations in the PSD shape. Typically, large γ values are associated with small particle dominated assemblages whereas large particles correspond to small γ values [*Loisel et al.*, 2006].

2.2. Statistical Analyses

[5] A pre-processing is applied to the time series of each grid point. Calendar months that are under-represented (less than 50% of occurrence) in the series are excluded, hence creating synthetic series with an annual cycle of varying length $P \leq 12$. Time series presenting more than 25% of missing data are discarded. The eventual remaining missing data are filled using the eigenvectors filtering method [*Ibanez and Conversi*, 2002].

[6] A time series X(t) (here the monthly series of γ and $b_{bp}(490)$) can be decomposed as $X(t) = S(t) + T(t) + I(t)$,

[1]Laboratoire d'Océanologie et de Géosciences, UMR CNRS LOG/ULCO 8187, Wimereux, France.
[2]European Commission-Joint Research Centre, Institute for Environment and Sustainability, Ispra, Italy.

0094-8276/11/2010GL046167

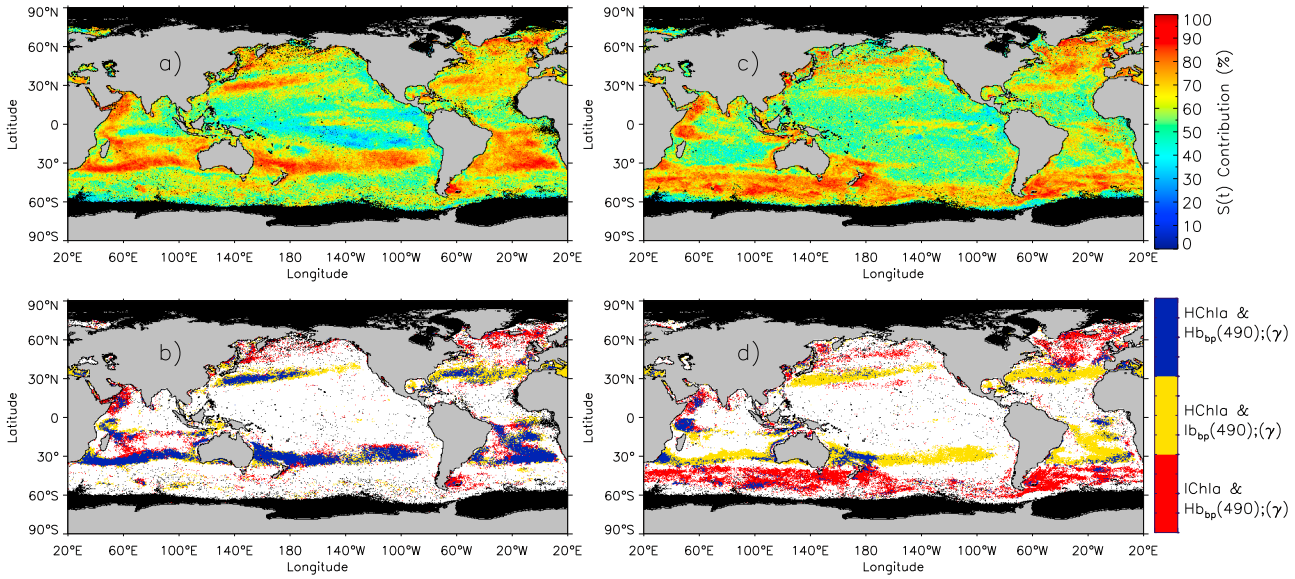

Figure 1. (a and c) Relative contribution of the Census X-11 seasonal term S(t) (in %) to the variance of the original time series for (a) particle backscattering spectral slope γ and (c) the particle backscattering coefficient at 490 nm, $b_{bp}(490)$. (b and d) Comparison of the seasonality patterns derived for the Chl*a* data [*Vantrepotte and Mélin*, 2009] and those obtained for (b) γ and (d) $b_{bp}(490)$. Points with a high contribution of S(t) to the variance of the Chl*a* series are in blue if the contribution of S(t) is also high for γ or $b_{bp}(490)$, yellow otherwise. Points with a low-to-moderate contribution of S(t) to the variance of the Chl*a* series are in red if the contribution of S(t) is high for γ or $b_{bp}(490)$, white otherwise. Seasonality is considered high if the percentage of variance explained by S(t) is larger than the global average plus 1 standard deviation (80%, 73% and 74% for Chl*a*, $b_{bp}(490)$ and γ, respectively).

where S, T and I represent, respectively, the seasonal, the trend-cycle, and the irregular (or residual) components. The time series decomposition is performed with the Census X-11 iterative band-pass filter algorithm that has been introduced for the analysis of sea surface temperature (SST) by *Pezzulli et al.* [2005] and of ocean-color data by *Vantrepotte and Mélin* [2009]. A major feature of the technique is that S(t) is defined locally in time, allowing year-to-year variations in the shape of the seasonal cycle. Consequently, the estimation of the trend-cycle term T(t) is not biased by the influence of inter-annual variations in seasonality [*Pezzulli et al.*, 2005]. The relative part of variance associated with the X-11 derived components S(t), T(t) and I(t) is estimated for each grid point in order to identify the main spatial patterns of temporal variability in the series. Additionally, the presence of monotonic long-term change in the data over the period investigated is assessed from the non-parametric seasonal Kendall statistics on X(t). This test, robust against non-normality, missing data and extreme values, accounts for the presence of seasonality in the series. The amplitude of the detected changes is evaluated by the non-parametric Sen's slope estimator [*Gilbert*, 1987] expressed in % yr^{-1}.

3. Results

[7] The γ series is characterized by the dominance of the seasonal signal S(t) in two mid-latitude zonal belts (~20°–40° latitude, Figure 1a) with a variance contribution >70%, contrasting with low seasonal contributions observed in large parts of the tropical ocean in association with relatively stable environmental conditions ([*Yoder and Kennelly*, 2003; *Vantrepotte and Mélin*, 2009] see auxiliary material for the contributions of I(t) and T(t)).[1] The seasonal contribution to the variance for γ globally reflects that described for Chl*a*, with some regional differences (Figure 1b) [*Vantrepotte and Mélin*, 2009]. Moreover, long-term monotonic changes in γ and Chl*a* (Figure 2a) are in general inversely related (even though the levels of significance and amplitudes of the respective trends might differ). Significant changes in γ ($p < 0.05$), with amplitudes reaching ±5% yr^{-1} are found in various regions, coincident with changes detected for Chl*a* (Figure 2b) [*Vantrepotte and Mélin*, 2009]. A positive γ signal is seen in the tropical Pacific, in the subtropical gyres of the Atlantic and Indian oceans, and in the Northeast Atlantic, while patterns of negative slopes include regions around Australia, the southern Arabian Sea, Pacific regions offshore North and South America and the Southeast Atlantic. Some areas depart from the inverse relation between γ and Chl*a* trends (such as some regions of the equatorial Pacific and Atlantic) which is in line with the regional variability in the slope and significance level of the log(Chl*a*) versus γ relationships reported by *Loisel et al.* [2006] (see also auxiliary material).

[8] Temporal patterns for $b_{bp}(490)$ differ from those reported for Chl*a* and seen for γ (Figure 1). The importance of seasonality in the $b_{bp}(490)$ signal is generally low (<50% of the total variance of the time series) in the entire tropical and subtropical domain, including in the regions of high seasonality for Chl*a* and γ (Figure 1c). In contrast, strong and stable seasonal fluctuations are found poleward of 45°,

[1] Auxiliary materials are available in the HTML. doi:10.1029/2010gl046167.

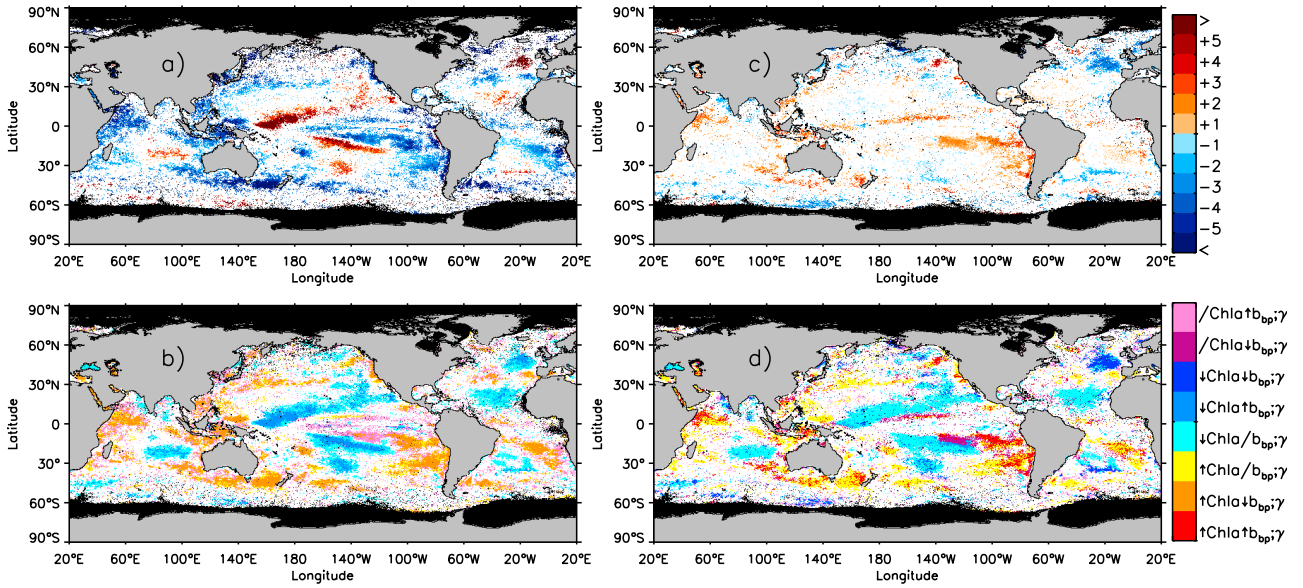

Figure 2. (a and c) Significant monotonic trends (seasonal Kendall test, $p < 0.05$, in % yr^{-1}) detected for (a) γ and (c) $b_{bp}(490)$. (b and d) Comparison between statistically significant trend slopes derived for Chl*a* and for (b) γ and (d) $b_{bp}(490)$. Eight categories are defined for points presenting an increasing Chl*a* associated with a positive (red), a negative (orange) or a non significant (yellow) trend slope for γ, those presenting a decreasing Chl*a* associated with a positive (summer-sky blue), a negative (dark blue) or a non significant (light-blue) trend slope for γ, and those with no significant trend in Chl*a* associated with a positive (pink), a negative (purple) or a non significant (white) trend slope for γ.

especially in the Southern Ocean, where high values and high spatio-temporal variability for b_{bp} have been pointed out [*Siegel et al.*, 2005; *Loisel et al.*, 2006]. As for Chl*a* and γ, the seasonal component of $b_{bp}(490)$ is generally stronger in the North Atlantic than in the North Pacific, this being consistent with the High-Nutrient Low-Chlorophyll conditions found in the latter [e.g., *Harrison et al.*, 1999]. A major difference with respect to Chl*a* and γ is seen for the long-term variations: the patterns of statistically significant change ($p < 0.05$) detected for $b_{bp}(490)$ are much fewer, most notably in the Northeast Atlantic and Southeast Pacific (with slopes varying from −3 to −4% yr^{-1}, and from +1 to +2% yr^{-1}, respectively, Figures 2c and 2d). These results suggest that, in spite of relevant changes in Chl*a*, the overall particle stock has remained fairly stable over the last decade for most of the ocean.

[9] The observation that the variations in Chla, γ and $b_{bp}(490)$ are very diversely related can be exemplified by two distinct situations. In the western tropical Pacific [150°W–155°E; 5°S–20°N], opposite changes have been found for Chl*a* and γ (Figures 2a and 2b). The X-11 trend-term T(t) indicates that these signals mostly result from sharp evolutions in 2000–2001, and that the inter-annual variations of these quantities have mirrored each other in this region ($r = -0.98$) (Figure 3). Moreover, T(t) for γ and Chl*a* and the time course of the Niño 4 index are well correlated ($r = +0{,}76$ and -0.78 respectively). This index, quantifying SST anomalies within the box 160°E–150°W, 5°S–5°N, reflects large scale oscillations in the physical environment; these in turn affect the regional phytoplankton biomass through their effect on the nutrient supply [e.g., *Behrenfeld et al.*, 2006]. The present results highlight that the changes in algal biomass are associated with concurrent shifts in particle size. Conversely, the regional average T(t) signal for $b_{bp}(490)$, and therefore the PM stock, has shown only a very slight decrease over the period with none of the large oscillations affecting Chl*a* or γ (Figure 3).

[10] The second example is the largest pattern of significant decrease (<−5% yr^{-1}) of $b_{bp}(490)$, observed in the Northeast Atlantic and accompanied by a similar decrease of Chl*a* and an increase of γ (Figure 4, 15°W–35°W; 45°N–55°N). The X-11 decomposition outputs also show that these variations are associated with a reduction of the amplitude of the seasonal fluctuations, particularly marked when comparing the time intervals 1997–2002 and 2002–2007 (Figure 4). Average S(t) seasonal maximum to minimum ratios computed before and after 2002 decrease by 54% and 72% for Chl*a* and $b_{bp}(490)$, respectively. Year-to-year variations in γ are in comparison less pronounced (−13% from 1997–2002 to 2002–2007). The patterns observed in this region can not be significantly related to climate indices characteristic of the Atlantic basin (e.g. North Atlantic

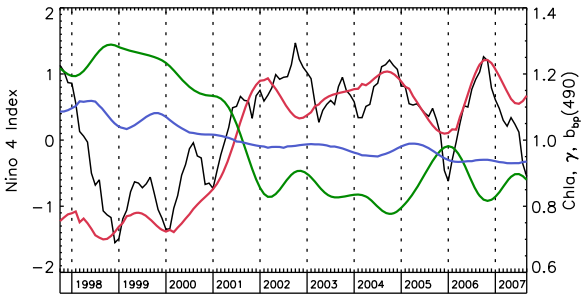

Figure 3. Ten year normalized (by the individual mean) regional average time series of $b_{bp}(490)$ (blue line), γ (red) and Chl*a* (green) in the western Pacific warm pool. The black line represents the SST Niño 4 index (http://www.cpc.ncep.noaa.gov/data/indices).

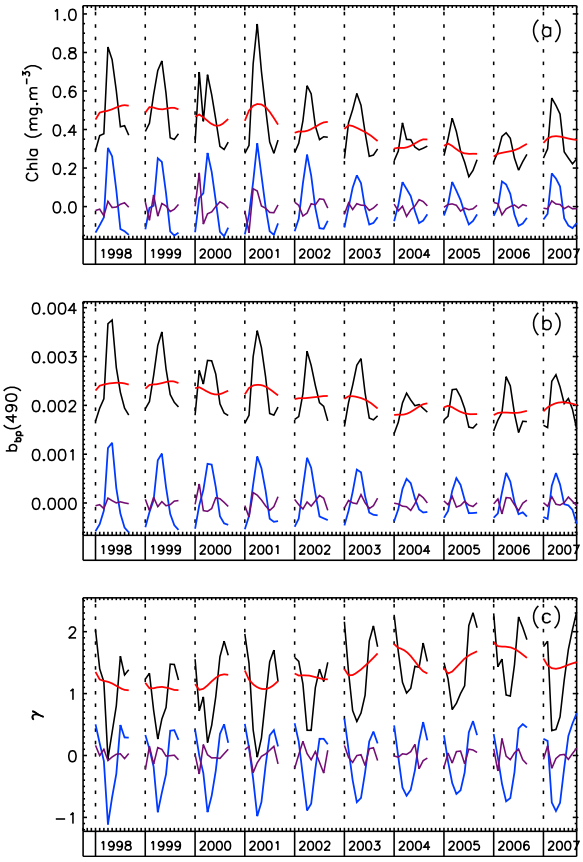

Figure 4. Regional averaged Census X-11 components: the original series X(t) (black line), the seasonal term S(t) (blue), the trend-cycle term (red), and the irregular term (violet), in the northeast Atlantic for (a) Chl*a* ($mg.m^{-3}$), (b) $b_{bp}(490)$ (m^{-1}) and (c) γ.

Oscillation, Atlantic Multi-decadal Oscillation indices) and will have to be explored through a dedicated analysis.

4. Conclusions

[11] Our results highlight the diversity of patterns characterizing the temporal variability of Chl*a*, $b_{bp}(490)$ (a proxy for particulate matter stock), and the particle backscattering spectral slope γ (an indicator for size distribution).

[12] Besides regional nuances, $b_{bp}(490)$ seasonal and inter-annual patterns appear weakly linked to those of Chl*a*. This is particularly true in the tropical ocean where the seasonal variations in $b_{bp}(490)$ may be driven by the net accumulation in the surface stratified layer of small-sized non-pigmented particles (including detritus, bacteria, colloids and viruses), which are not strictly co-varying with Chl*a* [*Loisel et al.*, 2002]. The lack of correlation [*Siegel et al.*, 2005] and/or temporal shift [*Loisel et al.*, 2006] between $b_{bp}(490)$ and Chl*a* documented in mid and low latitude regions has been also attributed to variations in the Chl*a*–to-carbon ratio due to temporal changes in the phytoplankton photo-acclimation [*Behrenfeld et al.*, 2005]. Finally, systematic variations in the relation between $b_{bp}(490)$ and POC can not be excluded.

[13] Conversely, seasonality and inter-annual signals generally have a similar spatial distribution for γ and Chl*a*. This suggests that the dynamics of phytoplankton and any covariates are important factors in defining the size spectrum of the PM assemblage. This result is consistent with the view that picoplankton-sized particles represent a biological background ubiquitously distributed in space and relatively stable in time [*Yentsch and Phinney*, 1989; *Kostadinov et al.*, 2009] that is episodically modulated by bloom events mainly caused by larger plankton organisms. In that respect, the variations displayed by Chl*a* and γ might be usefully completed by information on the spatio-temporal variations of phytoplankton functional types derived by other approaches [e.g., *Alvain et al.*, 2008].

[14] It is interesting to note that the variations in γ are at variance with those shown by $b_{bp}(490)$. The analysis presented above suggests that the variations associated with Chl*a* are sufficient to induce a significant shift in particle size but that is not always translated into a detectable (statistically significant) change in the PM stock as represented by $b_{bp}(490)$. For completeness, it is stressed here that the results obtained for b_{bp} do not depend on wavelength. Identifying the processes underlying this apparent discrepancy requires additional information not amenable to remote sensing, but these results may be reconciled by considering the definition of γ that makes it sensitive to slight changes in relative values of b_{bp} at several wavelengths. In other words, changes in b_{bp} specifically induced by variations in the spectral shape γ (i.e., independently of actual changes in amplitude of the entire spectrum due to a change in PM) are numerically small. This may be compounded for hyper-oligotrophic waters by a lower sensitivity of satellite measurements that could limit the performance of the inversion algorithms used to derive the amplitude of b_{bp} while derived spectral ratios are less affected. These elements likely concur to explain the relationship between b_{bp} and γ: below a certain b_{bp} value, the variations of b_{bp} are restricted to a narrow interval whereas γ still shows a large dynamic range (see auxiliary material).

[15] Ultimately, unraveling the links between the variations of $b_{bp}(490)$, γ and Chl*a* will require a comprehensive modeling that follows sources, sinks and nature of the organic material per particle size class, as it is affected by processes associated with grazing and microbial activity, aggregation and physical forcing.

[16] **Acknowledgments.** The authors thank the Ocean Biology Processing Group of NASA for the distribution of SeaWiFS data. We also thank the Agence Nationale de la Recherche for the financial support in the context of the GLOBPHY project. The authors thank the two anonymous reviewers for their valuable comments on the paper.

References

Alvain, S., C. Moulin, Y. Dandonneau, and H. Loisel (2008), Seasonal distribution and succession of dominant phytoplankton groups in the global ocean: A satellite view, *Global Biogeochem. Cycles*, *22*, GB3001, doi:10.1029/2007GB003154.

Aumont, O., E. Maier-Reimer, S. Blain, and P. Monfray (2003), An ecosystem model of the global ocean including Fe, Si, P colimitations, *Global Biogeochem. Cycles*, *17*(2), 1060, doi:10.1029/2001GB001745.

Behrenfeld, M. J., D. A. Siegel, C. R. McClain, E. S. Boss, and D. M. Shea (2005), Carbon-based ocean productivity and phytoplankton physiology from space, *Global Biogeochem. Cycles*, *19*, GB1006, doi:10.1029/2004GB002299.

Behrenfeld, M. J., R. T. O'Malley, D. A. Siegel, C. R. McClain, J. L. Sarmiento, G. C. Feldman, A. J. Milligan, P. G. Falkowski, R. M. Letelier, and E. S. Boss (2006), Climate-driven trends in contemporary ocean productivity, *Nature*, *444*, 752–755, doi:10.1038/nature05317.

Gilbert, R. O. (1987), *Statistical Methods for Environmental Pollution Monitoring*, John Wiley, New York.

Harrison, P. J., P. W. Boyd, D. E. Varela, S. Takeda, A. Shiomoto, and T. Odate (1999), Comparison of factors controlling phytoplankton productivity in the NE and NW subarctic gyres, *Prog. Oceanogr.*, *43*, 205–234, doi:10.1016/S0079-6611(99)00015-4.

Ibanez, F., and A. Conversi (2002), Prediction of missing values and detection of 'exceptional events' in a chronological planktonic series: A single algorithm, *Ecol. Modell.*, *154*, 9–23, doi:10.1016/S0304-3800(02)00033-9.

Kostadinov, T. S., D. A. Siegel, and S. Maritorena (2009), Retrieval of the particle size distribution from satellite ocean color observations, *J. Geophys. Res.*, *114*, C09015, doi:10.1029/2009JC005303.

Loisel, H., and D. Stramski (2000), Estimation of the inherent optical properties of natural waters from irradiance attenuation coefficient and reflectance in the presence of Raman scattering, *Appl. Opt.*, *39*, 3001–3011, doi:10.1364/AO.39.003001.

Loisel, H., D. Stramski, B. G. Mitchell, F. Fell, V. Fournier-Sicre, B. Lemasle, and M. Babin (2001), Comparison of the ocean inherent optical properties obtained from measurements and inverse modeling, *Appl. Opt.*, *40*, 2384–2397, doi:10.1364/AO.40.002384.

Loisel, H., J.-M. Nicolas, P.-Y. Deschamps, and R. Frouin (2002), Seasonal and inter-annual variability of particulate organic matter in the global ocean, *Geophys. Res. Lett.*, *29*(24), 2196, doi:10.1029/2002GL015948.

Loisel, H., J.-M. Nicolas, A. Sciandra, D. Stramski, and A. Poteau (2006), Spectral dependency of optical backscattering by marine particles from satellite remote sensing of the global ocean, *J. Geophys. Res.*, *111*, C09024, doi:10.1029/2005JC003367.

Martinez, E., D. Antoine, F. D'Ortenzio, and B. Gentili (2009), Climate-driven basin-scale decadal oscillations of oceanic phytoplankton, *Science*, *326*, 1253–1256, doi:10.1126/science.1177012.

Pezzulli, S., D. B. Stephenson, and A. Hannachi (2005), The variability of seasonality, *J. Clim.*, *18*, 71–88, doi:10.1175/JCLI-3256.1.

Reynolds, R. A., D. Stramski, and B. G. Mitchell (2001), A chlorophyll dependent semianalytical reflectance model derived from field measurements of absorption and backscattering coefficients within the Southern Ocean, *J. Geophys. Res.*, *106*, 7125–7138, doi:10.1029/1999JC000311.

Siegel, D. A., S. Maritorena, N. B. Nelson, and M. J. Behrenfeld (2005), Independence and interdependencies among global ocean color properties: Reassessing the bio-optical assumption, *J. Geophys. Res.*, *110*, C07011, doi:10.1029/2004JC002527.

Stramski, D., R. A. Reynolds, M. Kahru, and B. G. Mitchell (1999), Estimation of particulate organic carbon in the ocean from satellite remote sensing, *Science*, *285*, 239–242, doi:10.1126/science.285.5425.239.

Vantrepotte, V., and F. Mélin (2009), Temporal variability of 10-year global SeaWiFS time-series of phytoplankton chlorophyll a concentration, *ICES J. Mar. Sci.*, *66*, 1547–1556, doi:10.1093/icesjms/fsp107.

Yentsch, C. S., and D. A. Phinney (1989), A bridge between ocean optics and microbial ecology, *Limnol. Oceanogr.*, *34*, 1694–1705, doi:10.4319/lo.1989.34.8.1694.

Yoder, J. A., and M. A. Kennelly (2003), Seasonal and ENSO variability in global ocean phytoplankton chlorophyll derived from 4 years of SeaWiFS measurements, *Global Biogeochem. Cycles*, *17*(4), 1112, doi:10.1029/2002GB001942.

D. Desailly, L. Duforêt-Gaurier, H. Loisel, and V. Vantrepotte, LOG, CNRS-UMR 8187, 32 av. Foch, F-62930 Wimereux, France. (vincent.vantrepotte@univ-littoral.fr)

F. Mélin, European Commission-Joint Research Centre, Institute for Environment and Sustainability, TP272, Ispra I-21027, Italy.